



Performance of Jet Pulse Assembly with a Throttle Plate in a Fluidic Oscillator

Zhanhao Zhang¹, He Liu^{2*}, Jun Li¹, Rujun Huo², Chen Yu², Jianlong Wang², Zhiqiang Yu²

¹China University of Petroleum–Beijing, Beijing 102249, China

²CNPC Bohai Drilling Engineering Company Limited, Tianjin 300280, China

Corresponding Author Email: liuhe08@cnpc.com.cn

<https://doi.org/10.18280/ijht.380209>

ABSTRACT

Received: 18 December 2019

Accepted: 28 March 2020

Keywords:

fluidic oscillator, jet pulse assembly, structure optimization, pulse amplitude, field test

This paper aims to solve several defects of a 122mm fluidic oscillator in practical application, namely, unstable communication, high pressure drop, and low pulse amplitude. These defects were solved through mechanical analysis and field test. The results show that the downstroke piston rod can work smoothly, but the upstroke piston rod cannot due to the overcurrent resistance at the throttle plate. Through design optimization, the throttle plate can reduce the upward resistance, while increasing the pressure amplitude. Experiments indicate that the initial displacement of the new 122mm assembly was 5L/s. Under the displacement of 10–14L/s, the tool pressure drop fell between 1.5 and 3.5MPa, and the pulse amplitude reached 0.7–1.9MPa. The optimized tool clearly outperformed the original tool. The field tests demonstrate that the optimized tool could operate continuously for 155h without failure, and improve the drilling efficiency by 40.71%. The results fully verify the effectiveness of the optimized tool. The research results are conducive to the popularization of fluidic oscillator.

1. INTRODUCTION

The fluidic oscillator is a downhole tool to deal with the high friction and torque during the slide drilling of complex wells. Since its invention in the 2000s, this tool has been successfully applied in many oil fields [1, 2]. The fluidic oscillator can be divided into axial oscillation tools (AOTs) and lateral vibration tools (LVTs). Both reduce friction and torque by generating benign vibrations within the strings and downhole assembly [3].

By AOTs, pressure pulses are generated by changing the flow area of the mud through sliding or rotating valves, and converted into axial vibration by acting on the vibration assembly. By LVTs, a lateral vibration is produced with eccentric masses driven by mud. Both tools have been proven effective in complex wells, where AOTs perform better than LVTs [4, 5].

One of the most popular AOTs is an agitator oscillator invented by National Oilwell Varco (NOV) in 2002. Over the years, this AOT has been applied in thousands of oil wells to greatly improve the rate of penetration (ROP) [6]. However, the AOT involves complicated parts and moving structures, and requires strict follow-up maintenance, resulting in some failures in drilling projects.

Drawing on percussive and rotary drilling technology, Liu [7] designed a new drag and torque reduction tool called fluidic oscillator, in which the mud flows alternatively into a parallel path, under the control of bi-stable fluidic amplifiers with no moving part, to generate an intense pressure pulse. He et al. [8] analysed the feasibility of the fluidic oscillator, and implemented it to horizontal directional well drilling, using

computational fluid dynamic (CFD) simulations and experiments. Zhang et al. [9] compared the performance of fluidic oscillators without and with a throttle plate, and drew the following conclusions: the two designs produce different pressure drops and relative amplitudes, and the absence of a throttle plate effectively minimises the pressure drop of the oscillator. CNPC Bohai Drilling Engineering Company Limited [10] conducted several field drilling tests with a fluidic oscillator in complex wells, revealing that the fluidic oscillator is more than twice as efficient as conventional drilling tools, and could work for over 155h without failure in hot and corrosive environments.

However, the application scope of fluidic oscillator has been seriously bottlenecked by its high-pressure decrease in real-world scenarios, and the commutation and erosion problems of the fluidic amplifier [11]. Many scholars [12–14] have attempted to remove the bottleneck. Peng et al. [15] offered a mathematical model to characterise the wall-attaching jet flow in the bi-stable fluidic amplifier, and investigated the effect of actuator parameters on the critical flow velocity of a fluidic amplifier through CFD simulations. Based CFD simulations, many numerical methods have been developed to change the structure of the amplifier and reduce the pressure decrease [16–19].

This paper introduces the working principle and mechanical features of fluidic oscillator, optimizes the structural design of the oscillator, and analyses the defects in the oscillator structure. After that, the optimized and original tools were compared through field performance test, and the field application of the optimized tools was observed. The research results help to promote the application of fluidic oscillator.

2. MECHANICAL STRUCTURE AND DESIGN OPTIMIZATION

2.1 Mechanical principle

A fluidic oscillator mainly consists of a top axial oscillating assembly and a jet pulse assembly. The lateral structure is critical to the generation of intense pressure pulse. As shown in Figure 1, the jet pulse assembly contains the following components: an upper gland, a bi-stable fluidic amplifier, a cylinder, a piston, a throttle plate, to name but a few. The piston divides the cylinder into front and rear chambers.

When the jet pulse assembly works normally, the large-displacement mud flows into the assembly through the upper gland, where it is split into two parts. One part enters the fluidic amplifier to be turned into a jet with large kinetic energy, while the other flows into the spacer sleeve through the annulus flow channel, leading to jet wall attachment and switching in the amplifier [20, 21].

During wall attachment, the high-speed jet deflects to one side of the amplifier, and attaches to the side stably under the Coandă [22] effect. Then, the fluid enters one of the chambers of the cylinder via the output channel, causing the piston to move reciprocally. Due to the wall attachment, a pressure difference will appear between high pressure P_1 in the front chamber and the low pressure P_2 in the rear chamber, that is, the pressures of the two output channels. Therefore, the reciprocate motions of the piston are driven by the pressure difference of the output channels ($|P_1 - P_2|$).

During switching, once the piston reaches one of its stroke ends, a large high-energy pressure pulse will be created in the

signal channel above the output channel, owing to the piston-cylinder collision. With the growing pressure in the signal channel, the nozzle will eject a high-pressure control flow, pushing the jet switch to another side with low pressure. However, the jet might not successfully switch to another side, but remain on the middle position of the amplifier. To solve this problem, the collision force works together with the load in the throttle to drive the reverse motion of the position, making the jet to switch to the low-pressure side. By the time the control flow disappears, the pressure levels of front and rear chambers will reverse, causing piston to move in another stroke. This process of detachment and attachment continues, such that the position moves reciprocally under the periodic pulse.

As the oscillator moves up and downstrokes, the mud in the cylinder flows out from the emptying channel, and converges with the fluid shunted by the upper gland. Then, the mixture flows into the throttle plate through the outside path of the cylinder. When the oscillator actuates the piston to move reciprocally in the throttle plate, the cross-section area of the flow can be adjusted periodically in the taper hole of the throttle plate, and a periodic pressure pulsating can be produced with a certain amplitude.

As shown in Figure 1, the largest flow area and highest pressure (P_4) appear as the piston reaches the up dead centre. By contrast, the smallest flow area and lowest pressure (P_4') emerge as the piston moves to the down dead centre. Thus, the amplitude of pressure pulse can be defined as $P_4 - P_4'$, that is, the gap between the highest and lowest pressures in the throttle plate.

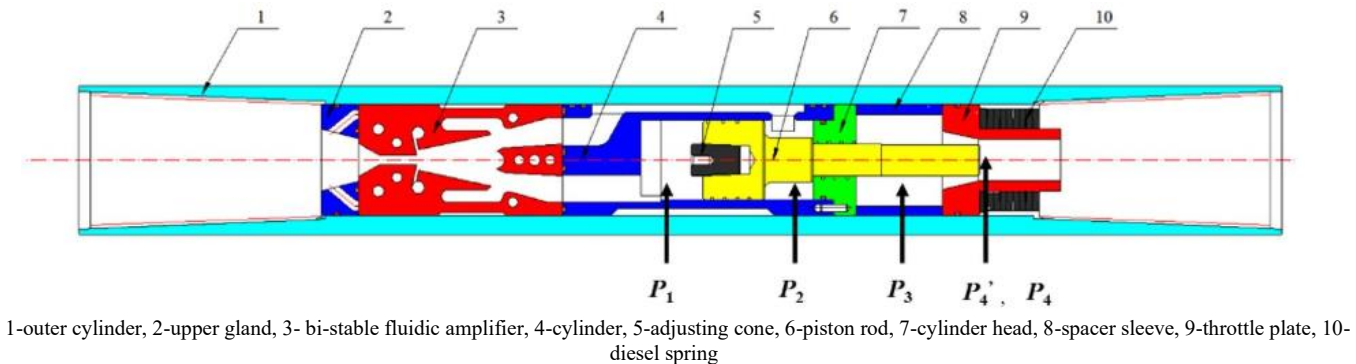


Figure 1. Mechanical structure of a jet pulse assembly in fluidic oscillator

2.2 Motion analysis

2.2.1 Up dead centre commutation

As shown in Figure 2, the transient stagnation of flow occurs as the piston moves to the dead centre. The ensuing pressure rise of the rear chamber will push the jet to the middle

position by the force of control flow (yellow jet core). Then, the pressure difference will disappear between the front and rear chambers ($P_1 \approx P_2 > P_3 > P_4$). According to the switching principle, the assisting effect of switching depends on the motion of the piston, calling for detailed force analysis.

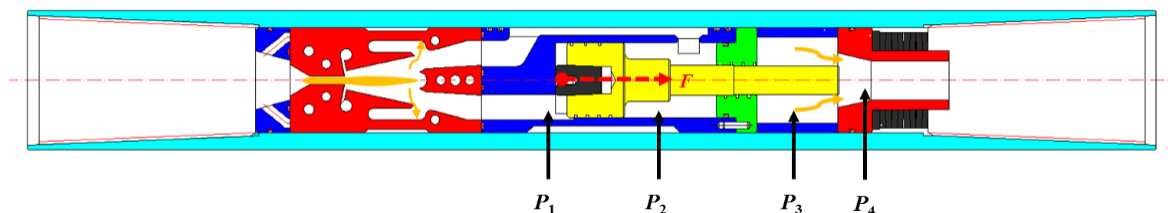


Figure 2. Up dead centre commutation

$$F \approx -m v_0 \quad (7)$$

As shown in Figure 2, the piston is subjected to three forces: the rebound force from the cylinder, the gravity of the piston, and the force at the throttle plate. After colliding into the cylinder, the piston will rebound. Let m , v_0 , and v_1 be the mass, pre-collision velocity, and post-collision velocity of the piston, respectively. Since the cylinder is assembled with an outer cylinder and drilling pipe, its mass M must be far greater than m . Suppose the cylinder moves at 0 and v_2 before and after the collision, respectively. Following the conservations of mechanical energy and momentum, we have:

$$m v_0 = m v_1 + M v_2 \quad (1)$$

$$\frac{1}{2} m v_0^2 = \frac{1}{2} m v_1^2 + \frac{1}{2} M v_2^2 \quad (2)$$

The solution can be expressed as:

$$v_1 = \frac{m - M}{m + M} v_0 \quad (3)$$

$$v_2 = \frac{2m}{m + M} v_0 \quad (4)$$

Given $M \gg m$, the solution can be rewritten as:

$$v_1 \approx -v_0 \quad (5)$$

$$v_2 \approx 0 \quad (6)$$

Thus, the piston moves reversely at the original velocity after the collision, and the rebound force on the piston can be calculated by:

where, F is a part of the force pushing the piston to downwards and the rebound force is proportional to the pre-collision velocity.

Normally, the mass of the piston is 8 kg, and the diameter of the inner cylinder is 64mm. Therefore, the gravity-induced pressure amounts to 0.02MPa, which is so small as negligible in engineering calculations.

In addition, as the piston moves to the up dead centre, its bottom is atop the throttle plate. This gives rise to an overcurrent pressure difference between the spacer and the throttle plate ($P_3 > P_4$). The pressure difference on the piston also pushes it to move downwards.

To sum up, the rebound force F and the force of the throttle plate are the resultant force that successfully push the piston to switch sides, which facilitates jet switching. This means the oscillator can work normally during the downstroke.

2.2.2 Downstroke motions

As shown in Figure 3, when the tool works during the downstroke, the jet attaches one side of the output channel with the front chamber. Then, the pressure P_1 quickly rises to surpass P_2 . Computation shows that pressure P_3 is greater than P_4 ($P_1 > P_2 > P_3 > P_4$). In this case, the piston is subjected to three forces: the force generated by the pressure difference between the front and rear chambers, the gravity of the piston, and the force at the throttle plate. Among them, the gravity is so small as to be negligible.

The force produced by the pressure difference of the cylinder points directly downward, so does the force on the throttle plate. As a result, the piston can move downwards steadily.

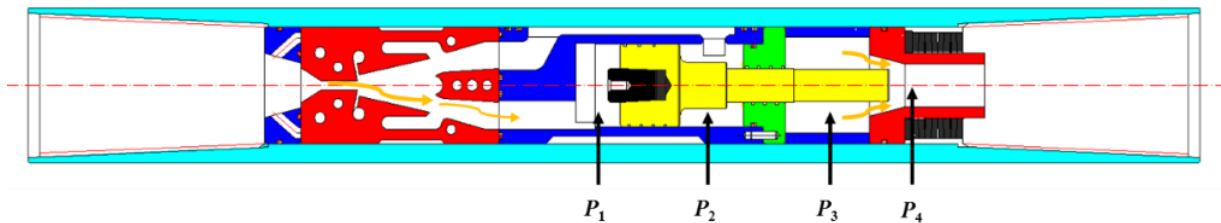


Figure 3. Downstroke motions

2.2.3 Analysis of down dead centre commutation

As shown in Figure 4, the piston works normally until it moves to the down dead centre, where it collides with the cylinder, and the jet detaches and switches to another side. The

pressure in the tool changes, causing the pressure to become $P_1 \approx P_2 > P_3 > P_4'$. Similarly, the force on the piston includes three parts: itself gravity, the rebound of the cylinder and the force at the throttle plate.

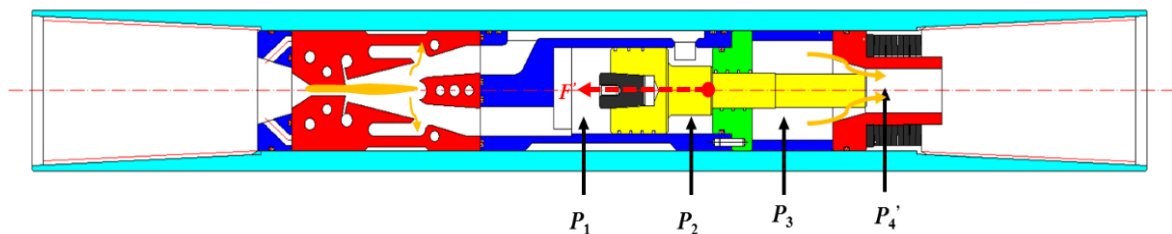


Figure 4. Down dead centre commutation

Without considering gravity, the rebound (F') points upwards, the direction of the next motion of the piston. However, the piston will be subjected to downward resistance, for the pressure difference (P_3-P_4') creates a downward force at the throttle plate. The piston cannot move upwards successfully, unless the rebound force surpasses the resistance.

In summary, the unstable performance of the tool is partly attributable to the downward resultant force, which cannot push the piston to move upwards, preventing the jet flow from completing the switch.

2.2.4 Upstroke motions

As shown in Figure 3, when the tool works during the upstroke, the jet attaches another side of the output channel with the rear chamber. The, the pressure P_2 quickly rises to surpass P_1 . Computation shows that pressure P_3 is greater than P_4 ($P_2 > P_1 > P_3 > P_4$). In this case, the piston is subjected to three forces: the force generated by the pressure difference between the front and rear chambers, the gravity of the piston, and the force at the throttle plate. Among them, the gravity is so small as to be negligible.

The force produced by the pressure difference of the cylinder points directly upward, opposite to the direction of the

force on the throttle plate. As a result, the piston can move upwards quickly at the beginning, and slows down to zero under the resistance from the throttle plate. This is the second reasons for the performance failure of the tool.

Through the above analysis, the oscillator failure in oil field application arises from two crucial reasons: First, the load of the throttle plate may be much larger than the rebound force, causing computing failure to the piston and the amplifier when the tool works on the down dead centre. Second, the overcurrent resistance from differential pressure prevents the piston from moving up.

In field applications, the oscillator failure can be prevented by increasing jet velocity. With the growing velocity of the jet flow, the amplifier erodes more quickly, and the pressure difference of the tool tends to increase. Another solution is to reduce the resistance from the throttle plant by increasing the flow area of the plate at the down dead centre. A larger flow area leads to higher pressure P_4' and smaller $P_4 - P_4'$, reducing the amplitude of the pressure pulse. However, these two solutions both have some defects. The oscillator structure should be redesigned to the problems in the down dead centre and upstroke.

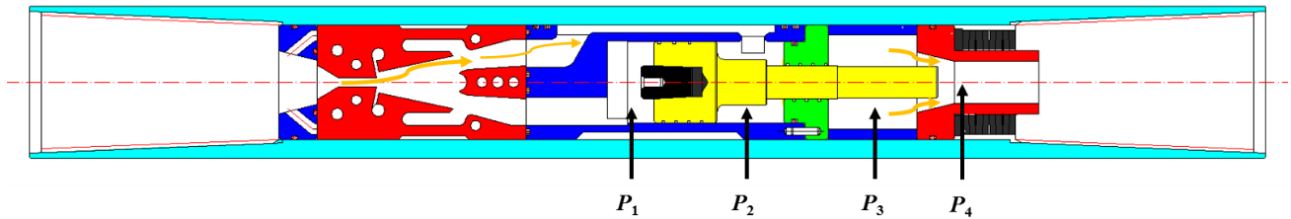
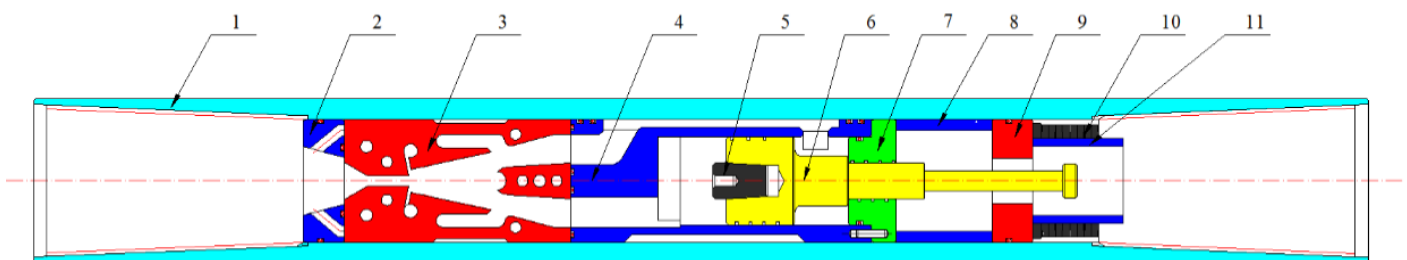


Figure 5. Upstroke motions

2.3 Design optimization

As shown in Figure 6, the authors redesigned the structure

of the throttle plate, without changing the other components. The new structure of the throttle plate can match with the reducing piston rod.



1-outer cylinder, 2-upper gland, 3-bi-stable fluidic jet amplifier, 4-cylinder, 5-adjusting cone, 6-piston rod, 7-cylinder head, 8-spacer sleeve, 9-throttle plate, 10-plate spring cover, 11-diesel spring

Figure 6. Optimized design of jet pulse assembly

2.3.1 Down and up dead centre commutations of the optimized structure

As shown in Figure 7, the flow area is maximized as the piston moves to the down dead centre, reducing the pressure difference (P_3-P_5') at the throttle plate. The reduction is followed by the decline in the resistance during piston switching. The optimized design makes it easy for the rebound force to exceed the resistance, such that the piston can facilitate the switching of the jet flow to another side.

As shown in Figure 8, the flow is is minimized, while the pressure difference (P_3-P_5) is maximized, when the piston is pushed downwards. Thus, the optimized design can ensure the effectiveness and success of down dead centre commutation.

In a word, the superiority of the optimized design for the throttle plate lies in that the flow area of the down dead centre and that of the up dead centre are respectively widened and narrowed, changing the resistance relationship and increasing the force to drive the downward motions of the piston.

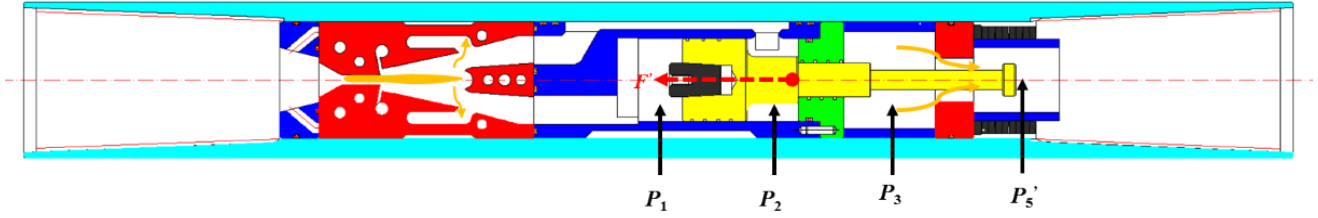


Figure 7. Down dead centre commutation

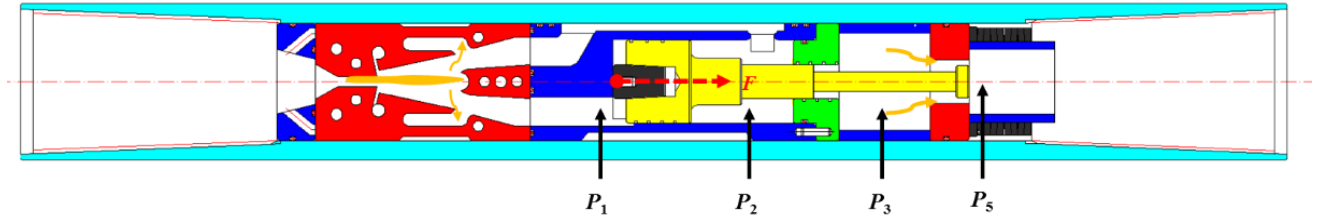


Figure 8. Up dead centre commutation

2.3.2 Upstroke motions of the optimized design

As the piston moves during the upstroke, the resistance becomes too large for the piston to move upwards successfully. Under the optimized design, the resistance does not increase when the piston moves up until it arrives at the up dead centre, where the resistance is the largest.

The critical condition of Eq. (9) is that power equals resistance:

$$\frac{(P_2 - P_1)}{(P_3 - P_5)} = \frac{(A_2 + A_3)}{A_1} \quad (10)$$

As shown in Eq. (10), the pressure difference ratio of power to resistance equals the area ratio between A_1 and $(A_2 + A_3)$. As long as the power remains constant, the resistance is positively correlated with the end area of the piston rod. Therefore, the diameter of the piston rod should be minimized without sacrificing the pressure amplitude.

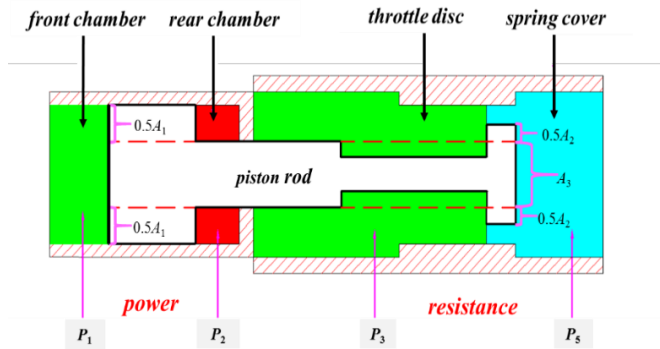


Figure 9. Upstroke motions

As shown in Figure 9, the total force on the piston can be expressed as:

$$\begin{aligned} F_t &= P_2 A_1 - P_1 (A_1 + A_3) - P_3 A_2 + P_5 (A_2 + A_3) \\ &= (P_2 - P_1) A_1 - (P_3 - P_5) (A_2 + A_3) \end{aligned} \quad (8)$$

where, F_t is the total force on the piston rod; P_1 , P_2 , P_3 and P_5 are the pressures on the related chambers; A_1 is the bottom area of the piston at the rear chamber; $(A_2 + A_3)$ is the end area of the piston rod at the spring cover; A_3 is the constant cross-sectional area of the piston.

It can be derived from Eq. (8) that when F_t is greater than zero, the piston can move stably upwards, provided that the power must surpass the resistance. Thus, Eq. (8) can also be expressed as:

$$(P_2 - P_1) A_1 \geq (P_3 - P_5) (A_2 + A_3) \quad (9)$$

3. EXPERIMENTS AND FIELD TEST

According to the optimized design, a jet pulse assembly (outer diameter: 122mm) was manufactured and assembled, and compared with the original tool through experiments. As shown in Figures 10–11, two pressure transducers were mounted on the inlet and outlet of the assembly, connecting the assembly with the data acquisition system and the computers. During the experiments, water was used as the drilling mud being pumped.

The inlet flow was monitored by a turbine flowmeter, which is controlled by an electric regulating valve. Once the mud pump and the piping system were ready, various amounts of drilling fluids were pumped into the jet pulse assembly, kicking off the working process.

Different rated volumes (5, 10, 12 and 14L/s) of the drilling mud were utilised to test the pressure drop of optimized and original structural tools under different displacement values. In the experiments, the optimized jet pulse assembly could work stably at all kinds of flow displacements, but the original tool could not work at the displacement of 5L/s.

In addition, field tests were conducted in North China oil fields to evaluate the effectiveness of the optimized jet pulse assembly. As shown in Figure 12, the optimized and original tools were adopted for slide drilling of six horizontal wells. The footage and the penetration rate were recorded to reveal the efficiency of speed increase of the same well.

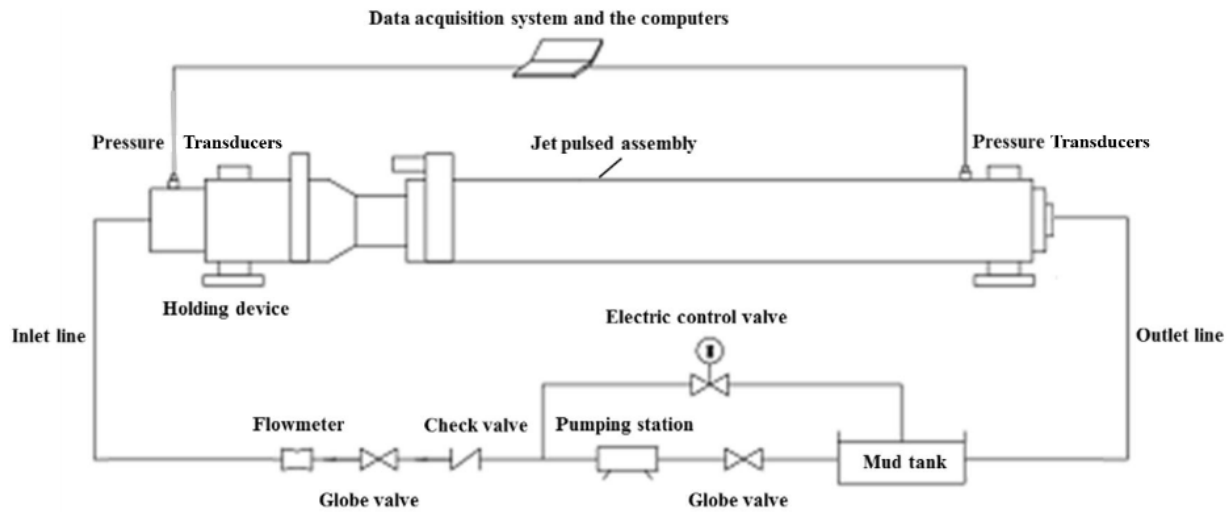


Figure 10. Experimental apparatus of the jet pulse assembly



Figure 11. Experiment with 122mm jet pulse assembly



Figure 12. Field test with 122mm jet pulse assembly

pulse is similar to a rectangular wave, for the flow area at the throttle plate of the optimized tool shows a sudden change. The pressure pulse of the optimized tool is more conducive to the rock-breaking by the drill bit.

In the original tool, the inlet pressure fell between 2.3 and 3.3MPa, and the outlet pressure fell between 0 and 0.4MPa. In the optimized tools, the inlet pressure varied from 2.6 to 3.8MPa, and the outlet pressure ranged from 0.6 to 1.0MPa. According to the previous definition, the pressure drop of a tool is the average pressure drop at the tool inlet and outlet; the pressure amplitude is the variation of the inlet pressure drop. Hence, for the displacement of 12L/s, the pressure drop and pressure pulse amplitude of the original tool were 2.6MPa and 1.0MPa, and those of the optimized tool were 2.4MPa and 1.2MPa, respectively. The optimized tool had greater amplitude and smaller pressure drop, revealing the effectiveness of tool optimization.

With the stepwise increase of the displacement flow, the pressure variations of all monitored sections in the original and optimized tools were recorded. As shown in Table 1, the original tool could not run at the displacement of 5L/s, but the optimized tool could run normally. This means the tool optimization can reduce the initial displacement of the tool.

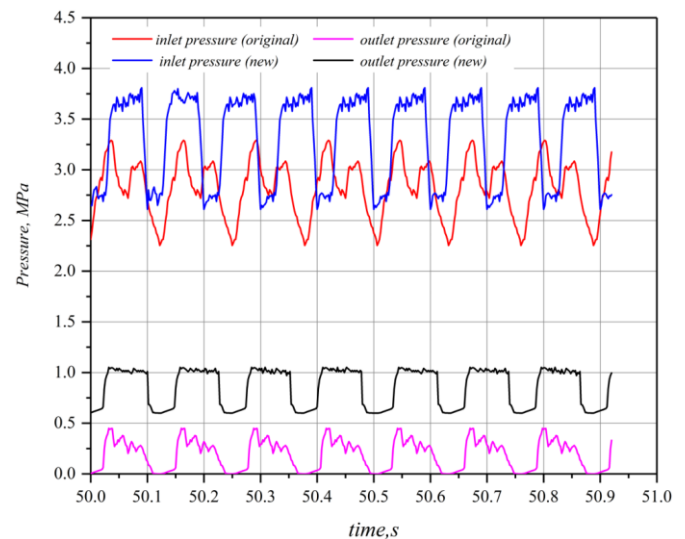


Figure 13. Pressure features of original and optimized jet pulse assemblies at 12L/s

4. RESULTS AND DISCUSSION

During the experiments, the working performances of the original and optimized tools were tested separately, including the inlet and outlet pressures. Considering the sheer volume of data, the performances were analysed with the test displacement of 12L/s below.

As shown in Figure 13, both tools worked normally during the experiments, producing periodic pressure pulse at the displacement of 12L/s. In the original tool, the pressure pulse is similar to a sine wave, for the conic flow area at the throttle plate changes gradually. In the optimized tool, the pressure

Table 1. Hydraulic features of the original and optimized tools at different displacements

	Displacement, L/s	Operation situation	Pressure drop, MPa	Pressure amplitude, MPa
Original tool	5	Run abnormally		
	10	Run normally	2.0	0.8
	12	Run normally	2.6	1.0
	14	Run normally	3.9	1.5
Optimized tool	5	Run normally	1.5	0.7
	10	Run normally	1.9	0.9
	12	Run normally	2.4	1.2
	14	Run normally	3.5	1.9

Experimental results show that the pressure drop and pressure amplitude of both tools increased almost exponentially with flow displacement (Figure 14).

As shown in Figure 15, the field tests on six wells were completed with the highest temperature reaching 134°C and the longest working time reaching 125 h. For each single well, the ROP achieved with the optimized tool was 26.84%–65.73% higher than that realized with the original tool. The average increase was 40.71%. In addition, the highest ROP stood at 13.54 m/h. After replacing the original tool with the optimized tool, the backing pressure of each well interval obviously reduces, the tool surface is stable, and the directional drilling is sustainable. The successful field applications demonstrate the effectiveness of the optimized 122mm jet pulse assembly.

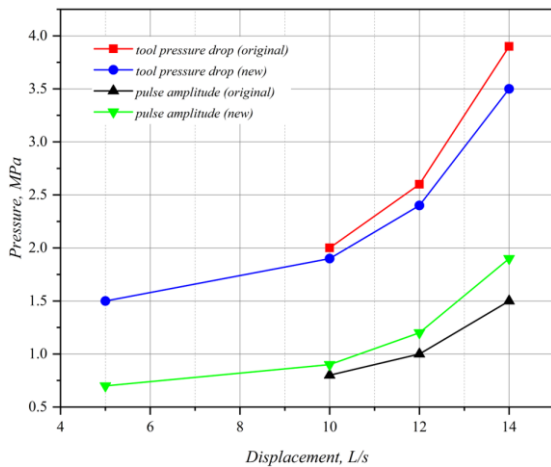


Figure 14. Variation in pressure drop and pressure amplitude of the two tools at different displacements

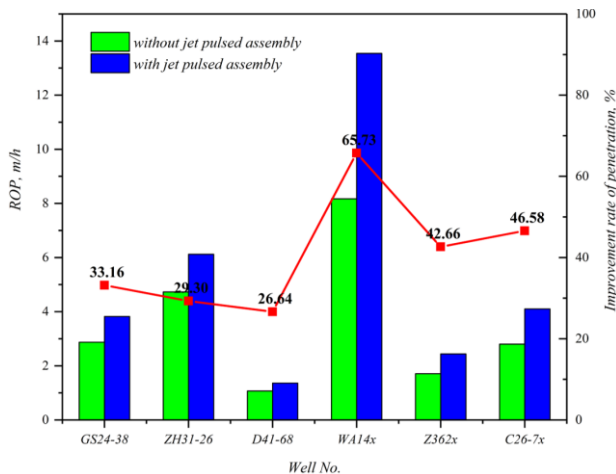


Figure 15. ROPs achieved by optimized and original tools and the single-well ROP increment

5. CONCLUSIONS

This paper introduces the working principle and mechanics of 122mm jet pulse assembly, and then optimizes the structural design of the throttle plate. The optimized tool was compared with the original tool through experiments and field tests. The main conclusions are as follows:

(1) During the downstroke, the piston rod of the original 122mm jet pulse assembly is subjected to two forces. One is the jet power of the front and rear chambers, and the other is the force produced by the pressure difference at the throttle plate. Under the two forces, the piston rod can move down steadily.

(2) During the upstroke, the piston rod is subjected to jet power and the resistance of over-current pressure difference at the throttle plate. The two forces work together to hinder the stable upward motion of the piston rod.

(3) The throttle plate was changed into a straight hole structure, and matched with a variable diameter piston rod. This alters the force relationship between the upstroke and the downstroke. During the downstroke, the power of the over-current pressure difference maximizes at the throttle plate, making the piston rod move down more stably. During the upstroke, the resistance of the over-current pressure difference is minimized at the throttle plate, so that the piston rod can move upwards more stably.

(4) Experiment results show that the initial displacement of the optimized 122mm jet pulse amplifier was 5L/s. As the inlet displacement changed within 5–14L/s, the drop pressure of the tool varied within 1.5–3.5MPa and the pressure amplitude ranged between 0.7 and 1.9MPa. The optimized tool had greater amplitude and smaller pressure drop, revealing the effectiveness of tool optimization. Field tests show that the optimized 122mm assembly can effectively improve the ROP of slide drilling and achieve a long service life. Hence, the optimized tool has a great potential for application in high-pressure horizontal wells with strong friction and resistance.

ACKNOWLEDGMENT

The study was supported by the Scientific Research and Technology Development Projects of CNPC (Grant No.: 2019D-4214), the Projects of CNPC Oilfield Service Company Limited (Grant No.: 2020T-002-006-2) and the Projects of CNPC Bohai Drilling Engineering Company Limited (Grant No.: 2018Z50Y).

REFERENCES

[1] Ermakov, K., Hampson, R., Barclay, D. (2020). Using fluidic oscillation technology with coiled tubing to

- cleanout scale from a high-pressure/extreme-temperature well beyond the limits of an HPHT motor: A case study from the UK North Sea. In SPE/ICoTA Well Intervention Conference and Exhibition. Society of Petroleum Engineers. <https://doi.org/10.2118/199825-MS>
- [2] Thomson, I. (2018). Successful creation of permanent reservoir isolation barriers using coiled tubing on the Norwegian continental shelf NCS. In SPE/ICoTA Coiled Tubing and Well Intervention Conference and Exhibition. Society of Petroleum Engineers. <https://doi.org/10.2118/189956-MS>
- [3] Liu, Y., Chen, P., Wang, X., Ma, T. (2016). Modeling friction-reducing performance of an axial oscillation tool using dynamic friction model. *Journal of Natural Gas Science and Engineering*, 33: 397-404. <https://doi.org/10.1016/j.jngse.2016.05.034>
- [4] Schmidt, H.J., Woszidlo, R., Nayeri, C.N., Paschereit, C.O. (2018). The effect of flow control on the wake dynamics of a rectangular bluff body in ground proximity. *Experiments in Fluids*, 59(6): 107. <https://doi.org/10.1007/s00348-018-2560-x>
- [5] Woszidlo, R., Ostermann, F., Schmidt, H.J. (2019). Fundamental properties of fluidic oscillators for flow control applications. *AIAA Journal*, 57(3): 978-992. <https://doi.org/10.2514/1.J056775>
- [6] Fu, B.W., Duanmu, Y., Wan, D.C. (2017). Vortex-induced vibrations of a flexible cylinder experiencing an oscillatory flow. In The twenty-seventh International Offshore and Polar Engineering Conference, San Francisco, California, USA.
- [7] Liu, H. (2014). Theoretical analysis and experimental research on liquid jet oscillation tool. (Doctoral dissertation, Ph. D. Thesis, Jilin University, Changchun, China).
- [8] He, J.F., Yin, K., Peng, J.M., Zhang, X.X., Liu, H., Gan, X. (2015). Design and feasibility analysis of a fluidic jet oscillator with application to horizontal directional well drilling. *Journal of Natural Gas Science and Engineering*, 27: 1723-1731. <https://doi.org/10.1016/j.jngse.2015.10.040>
- [9] Zhang, X., Peng, J., Liu, H., Wu, D. (2017). Performance analysis of a fluidic axial oscillation tool for friction reduction with the absence of a throttling plate. *Applied Sciences*, 7(4): 360. <https://doi.org/10.3390/app7040360>
- [10] CNPC Bohai Drilling Engineering Company Limited. (2016). BH-HVT jetting hydraulic oscillator for drilling; Technical Report; CNPC Bohai Drilling Engineering Company Limited: Tianjin, China.
- [11] Xue, L., Han, H., Wang, D., Liu, X.B., Liu, H., Yu, Z.Q. (2020). Experimental study on jet pulse assembly design and numerical simulation. *Petroleum Science*, 17(1): 222-231. <https://doi.org/10.1007/s12182-019-00396-y>
- [12] Aram, S., Lee, Y.T., Shan, H., Vargas, A. (2018). Computational fluid dynamic analysis of fluidic actuator for active flow control applications. *AIAA Journal*, 56(1): 111-120. <https://doi.org/10.2514/1.J056255>
- [13] Pandey, R.J., Kim, K.Y. (2018). Numerical modeling of internal flow in a fluidic oscillator. *Journal of Mechanical Science and Technology*, 32(3): 1041-1048. <https://doi.org/10.1007/s12206-018-0205-x>
- [14] Baghaei, M., Bergada, J.M. (2019). Analysis of the forces driving the oscillations in 3D fluidic oscillators. *Energies*, 12(24): 4720. <https://doi.org/10.3390/en12244720>
- [15] Peng, J.M., Yin, Q.L., Li, G.L., Liu, H., Wang, W. (2013). The effect of actuator parameters on the critical flow velocity of a fluidic amplifier. *Applied Mathematical Modelling*, 37(14-15): 7741-7751. <https://doi.org/10.1016/j.apm.2013.03.011>
- [16] Jeong, H.S., Kim, K.Y. (2018). Shape optimization of a feedback-channel fluidic oscillator. *Engineering Applications of Computational Fluid Mechanics*, 12(1): 169-181. <https://doi.org/10.1080/19942060.2017.1379441>
- [17] Zhang, X., Zhang, S., Peng, J., Wu, D. (2018). A fluidic oscillator with concave attachment walls and shorter splitter distance for fluidic DTH hammers. *Sensors and Actuators A: Physical*, 270: 127-135. <https://doi.org/10.1016/j.sna.2017.12.043>
- [18] Zhao, Y., Gong, P., Liu, Z., Wang, P., Feng, D., Tu, Y. (2018). Working Principle and Experimental Research of a New Type Fluidic Oscillator. *Fluid Machinery*, 46(9): 13-7,83.
- [19] Baghaei, M., Bergada, J.M. (2020). Fluidic Oscillators, the Effect of Some Design Modifications. *Applied Sciences*, 10(6): 2105. <https://doi.org/10.3390/app10062105>
- [20] Wang, Z., Xue, L. (2008). Hydraulic parameter model for design of fluidics downhole boost compressor. *Acta Petrolei Sinica*, 29(2): 308.
- [21] Wang, Z.M., Xue, L. (2007). Study on the attached flow and alteration flow character in fluidic element of down hole pressure intensifier. *Journal of Hydrodynamics (Ser. A)*, 3. 22(3): 352-357.
- [22] Coanda, H. (1936). Device for deflecting a stream of elastic fluid projected into an elastic fluid. United States Patent 2,052,869.